Optimized pulsed laser deposited barium ferrite thin films with narrow ferromagnetic resonance linewidths

Young-Yeal Song,[a] Sangita Kalarickal, and Carl E. Patton
Department of Physics, Colorado State University, Fort Collins, Colorado 80523

(Received 10 April 2003; accepted 18 July 2003)

Hexagonal *M*-type barium ferrite (BaM) films have been prepared by pulsed laser deposition. Optimal preparation conditions gave pure single phase films with the narrowest possible ferromagnetic resonance (FMR) linewidths. The films were deposited on *c*-plane sapphire substrates with a KrF excimer laser at wavelength of 248 nm and fluence of 1.7 J/cm^2. The minimum linewidth films were obtained for an oxygen partial pressure of 300 mTorr and a substrate temperature of 910 °C, and were 0.85 μm thick. X-ray diffraction indicated pure single crystal BaM phase with local *c*-axis deviations less than 0.15°. Vibrating sample magnetometry data gave hysteresis loops with minimal hysteresis and small coercive force, saturation induction $4\pi M_s$ of 4.2 kG and uniaxial anisotropy field H_A of 16.4 kOe. The H_A matches the anisotropy for bulk and the $4\pi M_s$ is about 10% below literature values for the bulk. The FMR spectra were measured from 50 to 75 GHz by shorted wave guide techniques with the static field perpendicular to the film. The optimized film uniform mode half power FMR linewidth at 60.3 GHz was 27 Oe. This linewidth was a linear function of the frequency with a response coefficient of 0.5 Oe/GHz and nearly zero frequency intercept. Within experimental error, this linewidth response is the same as for bulk crystals. The FMR spectra show additional standing spin wave (SSW) resonances which could be indexed to give field positions that scale with the square of index *n* except for low order modes. The scaling gave a standard exchange energy parameter, A_{ex}, of 6.4×10^{-7} erg/cm. The SSW linewidths scaled with n^2. Application of the Kittel thickness variation model to the SSW linewidth data gave an estimated thickness variation of the film of about 7%. © *2003 American Institute of Physics.* [DOI: 10.1063/1.1608475]

I. INTRODUCTION

One of the important challenges in the development of nonreciprocal millimeter wave devices for monolithic microwave integrated circuit (MMIC) applications is the production of thick, low loss hexagonal ferrite films.[1,2] Such films could be used to produce millimeter wave MMIC circulators and isolators, for example, with large figures of merit and low loss without the need for large biasing magnets. During the last decade, there has been considerable progress in this area. Several groups have demonstrated the fabrication of uniaxial *M*-type hexagonal barium ferrite (BaM) films with pulsed laser deposition (PLD) techniques.[3–11] Epitaxial BaM films grown by Dorsey *et al.*[3] had ferromagnetic resonance (FMR) half power linewidths of 114 Oe at 58 GHz. During the decade following this work, there was considerable effort by different groups to optimize various conditions to make films with low FMR linewidths.[5–11] Improvements in spin wave resonance characteristics of the BaM films were achieved by using a buffer layer between the substrate and the film.[7] The best BaM films were produced by Saraf *et al.* and they had FMR linewidths as low as 40 Oe at 58 GHz.[10,11] While low, such linewidths are still about 30% higher than the linewidths found in bulk single crystals.[12,13] These films, moreover, had thicknesses in the 1 μm range and were too thin for efficient devices. Attempts to produce thicker films resulted in stressed or cracked films with extremely large linewidths.[5]

The purpose of this work was to address the loss problem in PLD BaM films. The results demonstrate that one can produce good epitaxial films with microwave losses equal to those found in bulk crystals. The low loss films were produced with the basic PLD procedure documented in the literature.[4,11] The essential new element was in the careful optimization of deposition parameters, the use of a very low laser pulse rate during the initial stages of deposition, and a very slow cool down after deposition.

The best sample had a thickness of 0.85 μm and a half power main mode FMR linewidth of 27 Oe at 60.3 GHz. These main mode linewidths were linear in frequency with a response of 0.5 Oe/GHz and a zero linewidth intercept at zero frequency. This response was essentially the same as that previously reported for bulk single crystals. Analysis of the observed standing spin wave (SSW) modes gives a reasonable exchange energy coefficient in the 10^{-6} erg/cm range. The x-ray diffraction (XRD) pattern showed a hexagonal crystal structure with an extremely low crystallite orientation angular dispersion of 0.15°.

Section II describes the PLD sample preparation procedure and gives the conditions which were used to produce optimum low loss films. Section III gives results on the crystallographic and static magnetic properties. Sections IV and V give the microwave results. The overall FMR spectra and

[a]Electronic mail: yysong@lamar.colostate.edu

 © 2003 American Institute of Physics

Downloaded 20 Oct 2003 to 129.82.140.198. Redistribution subject to AIP license or copyright, see http://ojps.aip.org/japo/japcr.jsp

main FMR mode analysis are considered in Sec. IV. The standing spin wave modes are considered in Sec. V.

II. FILM PREPARATION

The PLD system was of standard design.[4] A pulsed excimer laser was used to ablate material from a target onto a substrate in a vacuum chamber with controlled atmosphere. The base vacuum pressure in the PLD chamber was 2.3×10^{-7} Torr. A 99.999% pure oxygen fill was used for the depositions and the cool down. Postdeposition annealing was always done in flowing pure oxygen at atmospheric pressure. The ablation was done with a KrF excimer laser at wavelength of 248 nm and stable single pulse energy held to $1.7\ \mathrm{J/cm^2} \pm 1\%$. The focused beam had an estimated spot size on the target of about $0.1\ \mathrm{cm^2}$. The beam was rastered over the target by a programmable mirror at a rate of 3 Hz. The target was also rotated at 15 rpm. The target was a 1 in. diam, 1/4 in. thick commercial $BaFe_{12}O_{19}$ disk produced by Target Material, Inc. The substrates were from MTI Corporation and consisted of small *c*-plane oriented 5 mm $\times$5 mm squares of 0.5 mm thick sapphire. The *c*-plane sapphire substrates have 7% lattice mismatch with BaM[6] and a coefficient of thermal expansion of $7.80 \times 10^{-6}\ ^\circ\mathrm{C}^{-1}$. This thermal expansion coefficient is 20% lower than that for BaM in the temperature range of $0-927\ ^\circ\mathrm{C}$.[14]

The control parameters for the depositions were (1) the sample target separation distance, (2) the laser pulse repetition rate, (3) the substrate temperature during deposition, (4) the oxygen pressure during deposition, (5) the total deposition time and corresponding film thickness, (6) the postdeposition cooling rate and oxygen pressure, and (7) the postdeposition annealing temperature and the heating/cooling rates. Based on literature descriptions of successful PLD BaM depositions, a total of 51 deposition runs were undertaken to do a systematic scan over the parameters stated above. The objective was to determine optimum conditions which would give films with the lowest possible microwave loss.

For each set of samples, the static magnetization versus the field was measured for in-plane and perpendicular-to-plane fields, and the FMR linewidth was measured from 50 to 75 GHz for perpendicular-to-plane fields only. For the films with good hysteresis loops and the lowest linewidths, the hexagonal structure and the orientation dispersion were examined by x-ray diffraction, and the thicknesses were measured from cross-sectional scanning electron microscopy images.

The sequence of depositions described above led to determination of the specific deposition conditions for films with very low linewidths. The optimum deposition and related conditions were as follows: (1) The sample target separation distance was 5 cm. (2) The laser pulse repetition rate was increased from 1 to 5 pulses per second (pps) in five equal steps over the first 5 min of deposition, followed by a rate of 10 pps for the remaining time. (3) The substrate temperature was held at 910 °C during deposition. (4) The oxygen pressure was held at 300 mTorr during deposition. (5) The deposition time for the lowest loss films was 20 min. (6) The postdeposition cooling rate was 2 °C/min and cooling was done in high purity oxygen at 400 Torr. (7) The postdeposition anneal was done in a tube furnace after removal of the sample from the PLD chamber. The sample was first heated from room temperature to 1100 °C at a rate of 10 °C/min, annealed for 20 min at the 1100 °C soak, and then cooled slowly back to room temperature at a rate of 2 °C/min. These conditions gave films in the 0.7–1.0 μm range. Thicker films were found to separate from the substrate during the annealing process. Presumably, this is due to different thermal expansion coefficients for BaM and sapphire.

The best films had smooth surfaces with a uniform reddish brown color and were semitransparent. Cross-sectional scanning electron microscopy (SEM) imaging indicated a lateral thickness variation of the film of a few percent. These optimized films had 60.3 GHz linewidths of about 27 Oe.

III. CRYSTALLOGRAPHIC AND STATIC MAGNETIC PROPERTIES

Crystallographic and static magnetic data are given below. These results provide clear and conclusive evidence of good epitaxial film quality with hexagonal structure and magnetic properties which match BaM.

The x-ray analysis was carried out at room temperature. Standard $\theta/2\theta$ source and detector scans were used to verify the hexagonal structure and *c*-axis orientation normal to the film plane. The *c*-plane (0008) diffraction line was then used for a rocking curve measurement to determine the *c*-axis angular dispersion. Finally, the $\theta/2\theta$ angles and sample tilt were set to detect diffraction from the (107) planes and the sample was rotated to check the hexagonal sixfold symmetry over the full area of the film.

Figure 1 shows representative XRD results for one particular 0.85 μm thick film obtained for the optimum PLD parameters listed above. Graph (a) shows a standard $\theta/2\theta$ diffraction scan, with the XRD intensity given on a log scale. The film was oriented such that the θ rotation gave a scattered beam that matched the specular reflection from the surface. For this setup, the detected diffraction peaks all come from *c*-plane scattering. The relevant (000ℓ) peaks are identified in Fig. 1(a), along with an ''S'' that identifies the single sapphire peak observed. The main graph in Fig. 1(b) shows a rocking curve for the (0008) peak in Fig. 1(a). The inset in Fig. 1(b) shows the intensity versus the in-plane sample rotation angle about the *c* axis for the (107) diffraction line.

The data in Fig. 1(a) show the expected *c*-plane diffraction peaks for a single crystal *c*-plane oriented BaM film. Except for the sapphire line, there are no additional peaks in the spectra. The strong (000ℓ) BaM peaks show that the film is single phase and has very good *c*-plane orientation. The full width at half maximum of the XRD rocking curve in Fig. 1(b) is 0.15°, and this width provides a quantitative measure of the *c*-axis dispersion. This small orientation dispersion provides further evidence that the film is epitaxial. The full $0^\circ-360^\circ$ angle scan in the graph (b) inset demonstrates further that the epitaxy is essentially texture free over the entire 3 sq mm probe beam area. The graph shows clear sixfold

Downloaded 20 Oct 2003 to 129.82.140.198. Redistribution subject to AIP license or copyright, see http://ojps.aip.org/japo/japcr.jsp

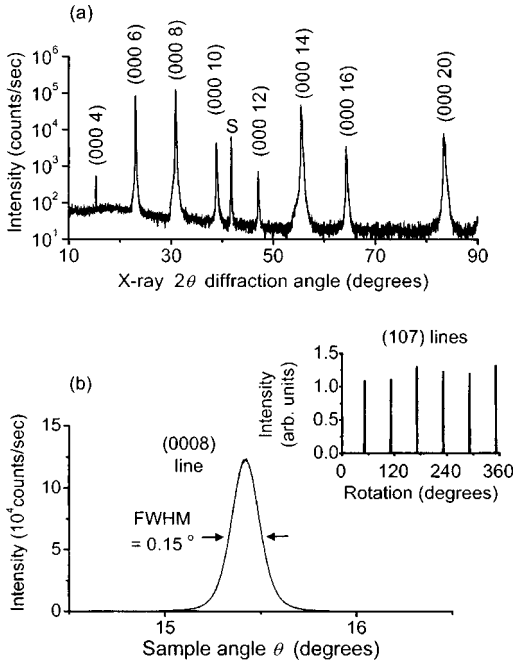

FIG. 1. X-ray diffaction data for the 0.85 μm thick BaM film. Graph (a) shows a standard $\theta/2\theta$ XRD scan. The sample orientation was such that the θ rotation matched the scattered beam to the specular reflection from the surface. The main graph in (b) shows a rocking curve for the (0008) diffraction line. The inset in (b) shows the XRD intensity versus the in-plane rotation angle for the diffraction line from (107) planes.

symmetry for the azimuthal in-plane angle scan over the (107) plane diffraction lines, just as one would expect for a texture free film.

The x-ray data provide clear evidence that the present BaM films are epitaxial c-plane films on c-plane sapphire. The films have very low crystallographic dispersion and no texture. The data given in Sec. IV will show that these epitaxial films also have magnetic and microwave properties which are very close to those of bulk BaM single crystals.

The static magnetization M was measured as a function of the static externally applied field H with a vibrating sample magnetometer at room temperature. Data were obtained for perpendicular-to-plane (PTP) and in-plane (IP) applied field configurations. The data were used to determine the saturation magnetization M_s and the effective uniaxial anisotropy field parameter H_A of the films. Based on uniaxial anisotropy energy density of the form $E_u = K_u \sin^2 \phi$, where K_u is the uniaxial anisotropy constant and ϕ is the angle between the saturation magnetization and the film normal, one can define an anisotropy field of $H_A = 2K_u/M_s$. A thin film with an easy axis normal to the film plane, like that for the present c-plane BaM samples, will be saturated at relatively low fields for the PTP field configuration and for fields above H_A for IP fields. Figure 2 shows representative magnetic induction $4\pi M$ versus field data for the same 0.85 μm thick film used for the x-ray analysis in Fig. 1. The graph shows results for both the PTP and the IP field configurations. The lines connecting the data points show simple spline fits. Data are shown for fields up to about 15 kOe.

The PTP data in Fig. 2 give narrow hysteresis loops with a coercive force of about 0.25 kOe, saturation at applied

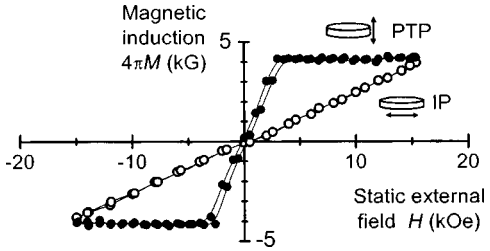

FIG. 2. Magnetic induction $4\pi M$ vs static external magnetic field H for the 0.85 μm thick film used for the data in Fig. 1. The field was applied perpendicular to plane or in plane. The points show the data and the lines show spline fits as a guide to the eye.

fields of about 3.3 kOe, and saturation $4\pi M$ values of about 4.2 kG. A fit to the saturation moment values gives $4\pi M_s = 4.2 \pm 0.12$ kG. The IP data show a linear magnetization versus field response at fields below 16 kOe or so and a corresponding slope of about 0.25 kG/kOe. The fitted slope is 0.256 kG/kOe. The extrapolated IP data intercept the high field PTP data at a field point which may be taken as the anisotropy field H_A. This intercept gives $H_A = 16.4 \pm 1.0$ kOe.

The small coercive force and relatively small saturation fields for the PTP data are related to domain considerations and indicative of the good single crystal film quality. The fitted saturation induction value of 4.2 kG is somewhat lower than literature values for bulk BaM single crystals, 4.7 kG.[12,13] The lack of any evident hysteresis and the linear rise in the magnetic induction with applied field for the PTP data provide two indications that the response is due to rotation processes only. The saturation point at $H_A = 16.4 \pm 1.0$ kOe for the IP data closely matches the expected anisotropy field for bulk BaM.[12,13] This further corroborates the IP response as due to gradual rotation of the magnetization to the in-plane direction.

Taken together, the crystallographic results and the static magnetic data show that these PLD films (1) have a hexagonal structure, (2) are c plane oriented with very little dispersion or texture, and (3) have $4\pi M_s$ and H_A values which are consistent with an M-type barium hexagonal ferrite. Section IV will show that these films also have exceptional microwave properties which match those of BaM single crystals, including the FMR linewidths which are essentially identical to those of the bulk.

IV. FMR SPECTRA AND MAIN MODE ANALYSIS

The ferromagnetic resonance absorption versus the static field at fixed frequency was measured from 50 to 75 GHz for the easy direction PTP field configuration. The actual data consisted of derivative profiles obtained by a standard field-swept shorted wave guide technique with ac field modulation and lock-in detection. A detailed description of the experimental setup and measurement technique is given in Ref. 15. Detailed data were obtained on the positions of the resonance lines, including both the main FMR response and the smaller standing spin wave modes, and the linewidths of the modes. The results shown below are for the same 0.85 μm thick film sample used for the results in Figs. 1 and 2.

Downloaded 20 Oct 2003 to 129.82.140.198. Redistribution subject to AIP license or copyright, see http://ojps.aip.org/japo/japcr.jsp

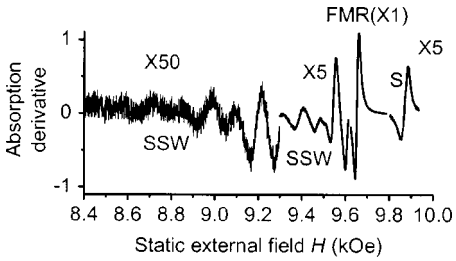

FIG. 3. Full ferromagnetic resonance and spin wave resonance absorption derivative vs static external field H for the 0.85 μm thick film at 60.3 GHz. Response regions above and below the main FMR mode are shown on an expanded vertical scale. The weak mode at a field above the FMR mode is labeled S to indicate a possible surface mode. The modes below the FMR mode are labeled SSW to indicate standing spin wave modes.

Figure 3 shows a typical result for the derivative of the absorbed power, shown in arbitrary but scaled units, versus the field over the entire range of observed resonances. These particular data are at 60.3 GHz. The vertical response for field regions below and above the FMR mode are shown on expanded scales. The main mode is labeled FMR mode, the weak mode above the FMR mode in the field is labeled S to indicate a possible surface mode, and the additional weak modes below the FMR mode in the field are labeled SSW to denote standing spin wave modes.

The spectrum in Fig. 3 demonstrates the essential features of the microwave response. (1) The main FMR peak is symmetric and quite narrow. (2) The spin wave modes are all relatively weak and expand outward as one moves towards lower fields. (3) There is a weak but well resolved possible surface mode above the FMR mode in the field. All of these results provide further indications of the good crystallographic and magnetic quality of the films. Further results below on the main mode profile, the main mode linewidth versus the frequency, and the spin wave mode positions and linewidths will expand these conclusions. With the exception of the narrow linewidths, the Fig. 3 data follow, more or less, the work cited in Sec. I.

Figure 4 shows the main FMR mode response data in Fig. 3 on an expanded field scale. The solid line shows a fit based on a Lorentzian absorption response with a center field position of 9653 Oe, a half power linewidth of 27 Oe, and a small positive offset of about 11%. This baseline shift was needed because of a small zero offset for the data. The vertical dashed lines delineate the negative to positive peak field width of 16 Oe for the derivative response. The fit in Fig. 3 is based on the Lorentzian form for absorbed power P_0,

$$P_0 = P_{0\,\max}\frac{(\Delta H_0/2)^2}{(H-H_0)^2+(\Delta H_0/2)^2}, \tag{1}$$

where $P_{0\,\max}$ denotes the peak in absorbed power at $H=H_0$ and H_0 and ΔH_0 denote the resonance field position and linewidth at half power, respectively. This same form, with 0 replaced by SSW mode indexing parameter n, will be used in Sec. V for analysis of the spin waves.

For purposes of this analysis, the derivative function dP_0/dH was written in the form of

$$\frac{dP_0}{dH} = -\frac{4P_{0\,\max}}{\Delta H_0}\frac{\left(\dfrac{H-H_0}{\Delta H_0/2}\right)}{\left[1+\left(\dfrac{H-H_0}{\Delta H_0/2}\right)^2\right]^2}. \tag{2}$$

Equation (2) is given here explicitly for two reasons. First, one can easily show that the extrema in Eq. (2) occur at $|H-H_0|/(\Delta H_0/2)=1/\sqrt{3}$. The separation in field between these extrema is equal to $\Delta H_0/\sqrt{3}$. This conversion is important for the linewidth analysis below and for comparisons with loss properties of other materials. Second, Eq. (2) shows that the actual peak values of $|dP_0/dH|$, taken as $B_{0\,\max}$, are equal to $3\sqrt{3}P_{0\,\max}/4\Delta H_0$. These scale with $P_{0\,\max}/\Delta H_0$. This means that the relative peak absorption values for the main resonance and the SSW resonances to be considered in Sec. V will be given by the corresponding $B_{0\,\max}\Delta H_0$ or $B_{n\,\max}\Delta H_n$ values for the modes. This will be an important consideration for the SSW mode analysis.

The data show that the main FMR mode response is highly symmetric and very sharp. The fit further shows that the experimental response is very close to that expected for a Lorentzian absorption line, except for some deviations on the low field wing. This deviation likely comes from the adjacent standing mode evident in Fig. 3. The fit also shows that the applicable half power linewidth is about 27 Oe. As noted, this corresponds to the peak-to-peak excursion width of 16 Oe in Fig. 4 multiplied by $\sqrt{3}$. Further linewidth data and discussion are given below. The standing spin wave mode response will also be considered shortly.

Figure 5 shows additional results on the half power FMR main mode linewidth as a function of the frequency. The circles show data for the same film used for the results presented above. The squares show published data on half power FMR linewidths for bulk single crystal BaM platelets from work by Karim *et al.*[12,16] The line shows a linear fit to all the data. The linear fit in Fig. 5 has a slope of 0.5 Oe/GHz and a zero frequency linewidth intercept of zero. While the film data show a fair amount of scatter, it is clear that the linewidths track the results for the bulk platelets. These data represent one of the key results of this work, namely, that the linewidth for the optimized PLD BaM films matches that of bulk single crystal BaM. The 0.5 Oe/GHz linewidth response is also significant. As a point of reference, note that the half

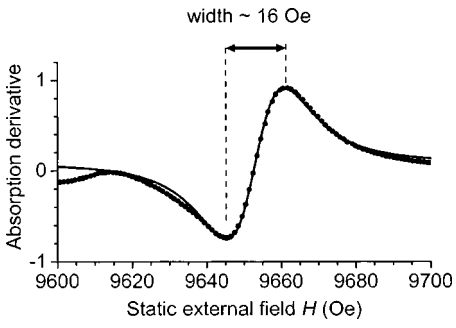

FIG. 4. Expanded view of the absorption derivative vs static external field H at 60.3 GHz for the main ferromagnetic resonance mode labeled FMR in Fig. 3. The closed circles show the data. The solid line shows a fit to the data based on a Lorentzian absorption response with resonance field of 9653 Oe, half power linewidth of 27 Oe, and 11% baseline shift.

Downloaded 20 Oct 2003 to 129.82.140.198. Redistribution subject to AIP license or copyright, see http://ojps.aip.org/japo/japcr.jsp

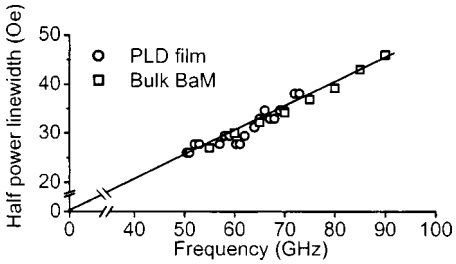

FIG. 5. Half power linewidth for the main ferromagnetic resonance mode vs the frequency. The circles show the data for the 0.85 μm thick PLD BaM film used for the results in previous figures. The squares show data from Ref. 12 for a bulk BaM single crystal platelet. The line represents a linear fit of all the data.

power FMR linewidth in single crystal yttrium–iron–garnet (YIG) typically has a response of 0.05 Oe/GHz and an extrapolated linewidth of zero at zero frequency. If the data in Fig. 5 are assumed to represent intrinsic losses, the response implies that such losses are a factor of 10 greater than those for YIG. Further results on the linewidths of the spin wave modes will be given below and they support this assumption.

V. SPIN WAVE MODE ANALYSIS

Turn now to the additional modes in Fig. 3. A full analysis of these modes in terms of surface anisotropy, pinning, mode indexing, and so on is beyond the scope of this article. The following has been done for this presentation. (1) The SSW modes were individually fitted to Lorentzian derivative response functions in the same way as in Sec. IV for the main mode. (2) The SSW mode field positions and linewidths were then indexed to give a good match to a linear H_n vs n^2 response. (3) Plots of H_n vs n^2 were then used to determine the exchange energy parameter for the film. (4) Plots of the mode linewidth as a function of n^2 were used to estimate possible thickness variations across the film area. The above analysis follows the procedures used by Shinde *et al.*,[7] Saraf *et al.*,[11] and others for standing spin wave modes in BaM films.[4,8] The results of (1)–(4) above are summarized below. A full surface anisotropy and pinning analysis of the surface and SSW modes for films is underway and will be published at a later date.

Table I gives the results of mode indexing and the H_n and ΔH_n values from the Lorentzian fits to the main mode and the SSW mode profiles in Fig. 3. There were 12 measurable modes. Column 1 shows the mode indices. The main mode is assigned $n=0$ to correspond to the uniform FMR mode. The other values correspond to the number of half wavelengths across the film thickness for the SSW modes that give linear H_n vs n^2 scaling. Columns 2 and 3 give the mode positions and linewidths. The fits to the data in Fig. 3 were done visually mode by mode with two iterations. In the first iteration, the mode field position, H_n, the mode linewidth, ΔH_n, the peak-to-peak derivative excursion, and the background level were adjusted to match the center portion of the experimental derivative response as closely as possible, starting with the strongest FMR mode and working down in field to the weaker modes. Once a rough fit to all the modes was obtained, this process was repeated. The second iteration was needed to take into account as much as possible the effect of adjacent modes on the response for a given fitted mode.

TABLE I. Tabulation of the assigned standing spin wave mode index n and the resonance field H_n values and half power linewidth ΔH_n values from Lorentzian derivative fits to the data of Fig. 3. The indexing was chosen to give linear scaling between H_n and n^2.

Standing spin wave mode index, n	Fitted mode field, H_n (Oe)	Fitted mode linewidth, ΔH_n (Oe)
0 (FMR)	9653±1	27±1
3	9607±2	33±2
5	9545±2	42±2
7	9474±2	60±5
8	9388±2	75±5
9	9295±2	90±20
10	9192±2	100±10
11	9075±5	80±20
12	8955±5	150±20
13	8830±10	150±30
14	8685±5	160±30
15	8540±10	200±30

As with the main mode fit, the main problem with the above H_n and ΔH_n fits was with the zero levels. These levels had to be adjusted to slightly different values for each mode fitted. These level shifts were on the order of 10% or less of the signal levels in each case. This problem is ascribed to drift in the zero level base line of the data. The uncertainties in the fitted H_n and ΔH_n values are indicated in Table I. They range from relatively small errors of 1 Oe or so for the strong modes to large errors of 10–50 Oe for the very weak modes.

The results in Table I provide a basis for two analyses. First, plots of H_n vs n^2 can be used to test the chosen indexing scheme and determine the applicable spin wave exchange stiffness parameter for c-direction spin waves. Second, plots of ΔH_n vs n or n^2 can be used to examine the wave number k dependence of the linewidth. Note that for SSW modes with n half wavelengths across film thickness L, the wave number is given by $k_n = n\pi/L$. In the work of Saraf *et al.*,[11] the BaM films had SSW fields and linewidths which both scaled with n^2. Similar results are obtained here.

The field positions of the SSW modes can be analyzed in terms of the spin wave dispersion relation for frequency ω_k versus wave number k for a wave vector parallel to the field. This relation may be written as

$$\omega_k = |\gamma| \left(H_n - 4\pi M_s + H_A + \frac{2A_{\mathrm{ex}}}{M_s} k_n^2 \right). \tag{3}$$

Here, γ is the gyromagnetic ratio and A_{ex} is the micromagnetic exchange energy coefficient defined through $E_{\mathrm{ex}} = -(A_{\mathrm{ex}}/M_s^2)\mathbf{M}(\mathbf{r},t)\cdot\nabla^2\mathbf{M}(\mathbf{r},t)$, where E_{ex} is the exchange energy density associated with nonparallel spins and $\mathbf{M}(\mathbf{r},t)$ is the position $\mathbf{r}$ dependent magnetization vector. The A_{ex} parameter for conventional ferromagnetic materials is typically in the range of 10^{-6} erg/cm and $|\gamma|/2\pi$ for BaM is close to the free electron value of 2.8 GHz/kOe. For fixed frequency and with all modes considered, the SSW mode

Downloaded 20 Oct 2003 to 129.82.140.198. Redistribution subject to AIP license or copyright, see http://ojps.aip.org/japo/japcr.jsp

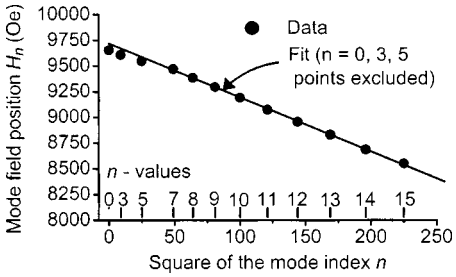

FIG. 6. Plot of mode field H_n vs the square of mode index n. The closed circles show data from Table I. The solid line shows a linear fit to the data with the $n=0$, 3, and 5 points excluded.

positions in the field, given by H_n, should start out at H_0 for $n=0$ and then decrease linearly in proportion to n^2 as the mode index advances. From Eq. (3), the slope of the H_n vs n^2 response should be equal to $2A_{ex}\pi^2/M_sL^2$.

Figure 6 shows a plot of H_n vs n^2 for the data in Table I. The actual n values for the modes plotted are shown along the bottom axis. The solid line shows a linear fit to these values with the $n=0$, 3, and 5 points excluded. The slope of the line fit is 5.25 Oe and the corresponding A_{ex} value according to Eq. (3) is 6.4×10^{-7} erg/cm. It should be noted that the three low order mode positions fall below the linear fit.

The results in Fig 6 show that the (0, 3, 5, 7, 8, 9, 10, 11, 12, 13, 14, 15) indexing scheme gives reasonable scaling of the mode positions with n^2 and an A_{ex} value which is close to the recent result given by Saraf *et al.*[11] Deviations from the n^2 response for $n=0$, 3, and 5 show that there are possible surface anisotropy and inhomogeneity effects present in the films.[17] Such effects are beyond the scope of this current work.

In a similar format, Fig. 7 shows the mode linewidth ΔH_n values from Table I as a function of n^2. The solid line shows the linear fit to these values, but with no points excluded from the fit. The slope of the line fit here is equal to 0.75 Oe and the intercept at $n^2=0$ is 20.4 Oe. These results indicate that the linewidths in BaM films increase with the square of wave number k and have the form $\Delta H=A+Ck^2$. This result is also consistent with the data of Saraf *et al.*[11]

Extensive SSW resonance data on metallic thin films[18,19] also give a quadratic ΔH vs k linewidth response. As noted

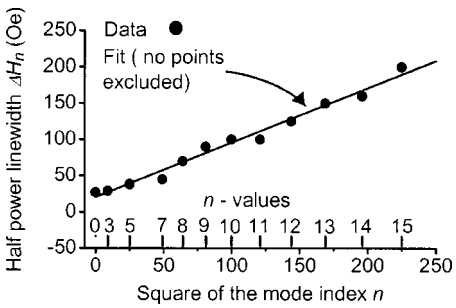

FIG. 7. Plot of mode linewidth ΔH_n vs the square of mode index n. The closed circles show data from Table I. The solid line shows a linear fit to the data with no points excluded.

in Ref. 11, this type of linewidth response can be explained by the Kittel surface pinning model in which the pinning, in combination with a small lateral variation in film thickness, serves to broaden the lines.[18] According to the Kittel model, lateral variations in thickness L over the film should result in variation of the local H_n values of the film for each of the modes. Since H_n scales with n^2, the line broadening, δH_n, due to these thickness variations would also vary with n^2. The observed linewidth would then be given by $\Delta H_n=\Delta H_0+\delta H_n$. For thickness variation of ΔL across the film, this thickness variation (TV) model gives a total linewidth of

$$\Delta H_n=\Delta H_0+\delta H_n=\Delta H_0+\left(\frac{2A_{ex}\pi^2}{M_sL^2}\right)\left(\frac{2\Delta L}{L}\right)n^2. \qquad (4)$$

From Eqs. (3) and (4), one can see that the fractional variation in thickness $\Delta L/L$ obtained from the TV model is equal to the slope of the ΔH_n vs n^2 response divided by twice the slope of the H_n vs n^2 response.

From the slopes of the line fits in Figs. 6 and 7, one obtains $\Delta L/L$ of about 7%. This fractional variation in thickness is consistent with the SEM cross-sectional data mentioned in Sec. II and the results from Ref. 11 for films prepared in a similar manner. For films with much smaller $\Delta L/L$, data of Shinde *et al.*[7] show half power 57 GHz SSW linewidths of about 104 Oe which are independent of mode index number n. These films were produced with a nonmagnetic hexagonal buffer layer between the BaM film and the substrate. If one assumes an upper limit linewidth uncertainty of 10% for the Ref. 7 data, one may estimate the resulting thickness variation in the films for this buffer layer technique to be below 1%. At the same time, the 104 Oe linewidths are somewhat larger than the smallest linewidths found here. Considered as a whole, the current results and those from Refs. 7 and 11 support the presence of $\Delta L/L$ in the low percent range for films made without a buffer layer and an inhomogeneously broadened linewidth which scales with the square of mode index n which stems from this lateral variation in thickness.

While this TV model explains very well the dominant quadratic response in Fig. 7, there are other issues which need to be considered. Any line broadening arising from a variation in thickness is likely to be dipole narrowed. In certain cases, magnetic dipole forces can decrease inhomogeneous broadening of the resonance linewidth. Even though a variation in thickness implies that different parts of the sample see different effective fields, the long range dipole interaction couples them together so that they assume a common resonance frequency. This would produce an additional factor on the order of $\delta H_n^2/M_s$ and give much smaller linewidth broadening than that predicted by the TV model. This would also change the scaling from n^2 to n^4.

Besides the above dipole narrowing effect, it may also be necessary to consider three magnon processes which give rise to a linewidth with a linear wave number k dependence. Spin wave linewidth measurements in low linewidth YIG in both bulk and thin film form are known to exhibit a linear k-dependent linewidth of the form $\Delta H=A+Bk$.[20–23] This $\Delta H=A+Bk$ form has a reasonable basis in theory, and has been explained in terms of intrinsic three magnon

Downloaded 20 Oct 2003 to 129.82.140.198. Redistribution subject to AIP license or copyright, see http://ojps.aip.org/japo/japcr.jsp

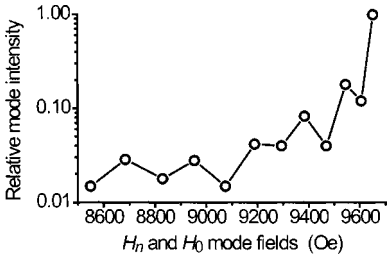

FIG. 8. Plot of the derivative maximum linewidth product $B_{n\,\max}\Delta H_n$ normalized to the corresponding $B_{0\,\max}\Delta H_0$ product for the main mode as a function of mode field H_n, all based on Lorentzian fits to the data in Fig. 3. The upper right corner point, at a relative peak absorption value of unity and field H_0, is for the main mode.

processes.[24] A preliminary analysis indicates that such processes may be valid for the present BaM films. Clearly, there are a number of issues which still need to be resolved in order to provide a full explanation of the SSW mode linewidths in BaM films.

One final consideration involves mode intensities. The strengths of the modes can provide an indication of the order of the mode and the nature of the pinning. For a uniform microwave excitation field, as is the case here, a uniform mode with $n=0$ or a fully pinned mode with an odd number of SSW half wavelengths across the film would result in relatively strong absorption, while an even number of half wavelengths should give a weak response. From the equations in Sec. IV, it was shown that the peak absorption for a given mode should scale with $B_{n\,\max}\Delta H_n$, the product of the linewidth and the value of the derivative maxima. These fits provide, therefore, a ready way by which to compare intensities.

Figure 8 shows a mode-to-mode comparison of the peak absorption values for the uniform mode and the SSW signals at lower fields. This comparison is shown as a plot of the $B_{n\,\max}\Delta H_n$ product, normalized to $B_{0\,\max}\Delta H_0$, as a function of H_n. All parameters are derived from the Lorentzian fits to the data in Fig. 3. The upper right corner point at a relative peak absorption value of unity is for the uniform mode. The lines between the points provide a guide to the eye.

The data in Fig. 8 show evidence of high-low-high mode-to-mode variation in the strengths of the resonances which are qualitatively in accord with a pinning model. Completely pinned SSW modes with zero dynamic magnetization at the film surfaces and an integral number of half wavelengths across the film would show spectra for which the odd mode intensities gradually fall off with increasing n and no even mode signals. Films with some reduced degree of surface anisotropy would show strong odd modes and weak even modes. The behavior in Fig. 8, with a gradual falloff in intensity and a weak odd–even effect, indicates rather strong surface anisotropy but a lack of complete pinning. This is consistent with the distinct surface mode resonance well above the main mode in field shown in Fig. 3.

The behavior in Fig. 8 indicates that the best approach to quantitative analysis of the SSW mode positions and linewidths is through full surface anisotropy treatment. As noted above, the three strongest modes fall below the H_n vs n^2 fit in Fig. 6. The shifts in the low order mode fields relative to the quadratic n response can provide a good indication of any sign of surface anisotropy, the effect of variations in magnetization across the film, etc. These effects are well documented for SSW modes in metallic thin films and to some extent[25–27] for YIG. Further work on a full SSW analysis of PLD BaM films is in progress.

VI. SUMMARY

High quality single crystal barium hexaferrite films have been fabricated on sapphire substrates by pulsed laser deposition. The key to high quality is the use of a very low laser pulse rate during the initial stages of deposition and a very slow cool down. The half power ferromagnetic resonance main mode linewidths for the best films was 27 Oe at 60.3 GHz. The linewidth was a linear function of the frequency with response of 0.5 Oe/GHz and showed zero linewidth intercept at zero frequency. These linewidths matched linewidths for bulk single crystal BaM platelets.

The spectra also exhibited distinct weaker resonance well above the main mode and a sequence of standing spin wave mode resonances at lower fields. It was possible to obtain an indexing sequence for the SSW modes, based on the assumption of an integral number n of half wavelengths across the film cross section, which yielded mode field positions (H_n) and mode linewidths (ΔH_n) which scaled with n^2. Following the work of Saraf *et al.*,[11] the H_n vs n^2 response gave an exchange energy coefficient $A_{\rm ex}$ in the 10^{-6} erg/cm range and is in agreement with previous work. Also following Refs. 11, 18, and 19, the ΔH_n vs n^2 data were analyzed in terms of a simple thickness variation model. If there is variation in thickness over the film area, and if there is no dipole narrowing, there will be additional line broadening as the field position for a given mode changes from point to point. As in Ref. 11, this model gave a possible thickness variation in the 10% range.

Further data on mode intensities indicated that simple indexing approaches can provide only a qualitative assessment of the SSW mode properties, and that a full analysis in terms of surface anisotropy is needed. Such work is in progress.

ACKNOWLEDGMENTS

This work was sponsored in part by the Office of Naval Research under Grant Nos. N00014-94-1-0096 and N00014-03-1-0070, the National Science Foundation under Grant Nos. DMR-9801649 and DMR-0108797, and the Institute for Basic Sciences, Chungbuk National University, Cheongju, Korea. Advice and assistance from Dr. Vincent Harris of the Naval Research Laboratory, Professor R. Ramesh and Dr. R. D. Vispute of the University of Maryland, and Dr. Steven A. Oliver of Northeastern University are gratefully acknowledged. One of the authors (S.K.) is particularly grateful to Professor Ramesh for making his facility available to her during her one month visit, to Dr. L. V. Saraf for providing her with training on the PLD system, and to Dr. Vispute for valuable discussions.

Downloaded 20 Oct 2003 to 129.82.140.198. Redistribution subject to AIP license or copyright, see http://ojps.aip.org/japo/japcr.jsp

[1] S. A. Oliver, P. Shi, W. Hu, H. How, S. W. McKnight, N. E. McGruer, P. M. Zavracky, and C. Vittoria, IEEE Trans. Microwave Theory Tech. **49**, 385 (2001).
[2] P. Shi, H. How, X. Zuo, S. D. Yoon, S. A. Oliver, and C. Vittoria, IEEE Trans. Magn. **37**, 2389 (2001).
[3] P. Dorsey, R. Seed, C. Vittoria, D. B. Chrisey, C. Carosella, P. Lubitz, and J. S. Horwitz, IEEE Trans. Magn. **28**, 3216 (1992).
[4] C. A. Carosella, D. B. Chrisey, P. Lubitz, J. S. Horwitz, P. Dorsey, R. Seed, and C. Vittoria, J. Appl. Phys. **71**, 5107 (1992).
[5] P. C. Dorsey, D. B. Chrisey, J. S. Horwitz, P. Lubitz, and R. C. Y. Auyeung, IEEE Trans. Magn. **30**, 4512 (1994).
[6] S. R. Shinde, R. Ramesh, S. E. Lofland, S. M. Bhagat, S. B. Ogale, R. P. Sharma, and T. Venkatesan, Appl. Phys. Lett. **72**, 3443 (1998).
[7] S. R. Shinde, S. E. Lofland, C. S. Ganpule, S. M. Bhagat, S. B. Ogale, R. Ramesh, and T. Venkatesan, Appl. Phys. Lett. **74**, 594 (1999).
[8] S. R. Shinde, S. E. Lofland, C. S. Ganpule, S. B. Ogale, S. M. Bhagat, T. Venkatesan, and R. Ramesh, J. Appl. Phys. **85**, 7459 (1999).
[9] S. A. Oliver, S. D. Yoon, I. Kozulin, M. L. Chen, and C. Vittoria, Appl. Phys. Lett. **76**, 3612 (2000).
[10] L. V. Saraf, S. E. Lofland, A. V. Cresce, A. P. Monga, S. M. Bhagat, and R. Ramesh, IEEE Trans. Magn. **37**, 2377 (2001).
[11] L. V. Saraf, S. E. Lofland, A. V. Cresce, S. M. Bhagat, and R. Ramesh, Appl. Phys. Lett. **79**, 385 (2001).
[12] R. Karim, K. D. McKinstry, J. R. Truedson, and C. E. Patton, IEEE Trans Magn. **28**, 3225 (1992).
[13] M. A. Wittenauer, J. A. Nyenhuis, A. I. Schindler, H. Sato, F. J. Friedlaender, J. Truedson, R. Karim, and C. E. Patton, J. Cryst. Growth **130**, 533 (1993).
[14] P. C. Dorsey, S. B. Qadri, J. L. Feldman, J. S. Horwitz, P. Lubitz, D. B. Chrisey, and J. B. Ings, J. Appl. Phys. **79**, 3517 (1996).
[15] S. V. Lebedev, C. E. Patton, M. A. Wittenauer, L. V. Saraf, and R. Ramesh, J. Appl. Phys. **91**, 4426 (2002).
[16] R. Karim, S. D. Ball, J. R. Truedson, and C. E. Patton, J. Appl. Phys. **73**, 4512 (1993).
[17] F. Schreiber and Z. Frait, Phys. Rev. B **54**, 6473 (1996).
[18] T. G. Phillips and H. M. Rosenberg, Phys. Lett. **8**, 298 (1964).
[19] H. Pascard and F. Hoffmann, IEEE Trans. Magn. **7**, 764 (1971).
[20] C. E. Patton, Phys. State. Sol. **92**, 14 (1979).
[21] C. E. Patton, Phys. State. Sol. **93**, 63 (1979).
[22] C. E. Patton and W. Jantz, IEEE Trans. Magn. **14**, 698 (1978).
[23] C. E. Patton and W. Jantz, J. Appl. Phys. **50**, 7082 (1979).
[24] M. Sparks, *Ferromagnetic Relaxation Theory* (McGraw–Hill, New York, 1964).
[25] M. H. Seavey, Jr. and P. E. Tannenwald, Phys. Rev. Lett. **1**, 168 (1958).
[26] M. Sparks, B. R. Tittmann, J. E. Mee, and C. Newkirk, J. Appl. Phys. **40**, 1518 (1969).
[27] P. E. Wigen, T. S. Stakelon, H. Puszkarski, and P. Yen, AIP Conf. Proc. **29**, 670 (1976).

Downloaded 20 Oct 2003 to 129.82.140.198. Redistribution subject to AIP license or copyright, see http://ojps.aip.org/japo/japcr.jsp